Mon. Not. R. Astron. Soc. **000**, 1–5 (2014) Printed 6 May 2014 (MN LATEX style file v2.2)

Dark matter-baryons separation at the lowest mass scale: the Bullet Group⋆

F. Gastaldello[1,2]†, M. Limousin[3,4], G. Foëx[5], R. P. Muñoz[6], T. Verdugo[7], V. Motta[5], A. More[8,9], R. Cabanac[10], D. A. Buote[2], D. Eckert[11,1], S. Ettori[12,13], A. Fritz[1], S. Ghizzardi[1], P. J. Humphrey[2], M. Meneghetti[12,13,14], M. Rossetti[15,1]

[1] *INAF - IASF Milano, via E. Bassini 15, I-20133 Milano, Italy.*
[2] *Department of Physics and Astronomy, University of California at Irvine, 4129 Frederick Reines Hall, Irvine, CA 92697-4575, USA*
[3] *Aix Marseille Universit, CNRS, LAM (Laboratoire d Astrophysique de Marseille), UMR 7326, 13388, Marseille, France*
[4] *Dark Cosmology Centre, Niels Bohr Institute, University of Copenhagen, Juliane Maries Vej 30, DK-2100 Copenhagen, Denmark*
[5] *Instituto de Física y Astronomía, Universidad de Valparaíso, Avda. Gran Bretaña 1111, Valparaĩso, Chile*
[6] *Instituto de Astrofísica, Facultad de Física, Pontificia Universidad Católica de Chile, Av. Mackenna 4860, 7820436 Macul, Santiago, Chile*
[7] *Centro de Investigaciones de Astronomía, AP 264, Mérida 5101-A, Venezuela*
[8] *Kavli Institute for Cosmological Physics, U. of Chicago, 5640 S. Ellis Ave., Chicago IL-60637, USA*
[9] *Kavli IPMU, U. of Tokyo, 5-1-5 Kashiwanoha, Kashiwa, 277-8583, Japan*
[10] *Universite de Toulouse-UPS, CNRS; Institut de Recherche en Astrophysique et Planetologie; 57 avenue d Azereix, 65000 Tarbes, France*
[11] *Astronomical Observatory of the University of Geneva, ch. d Ecogia 16, 1290 Versoix, Switzerland*
[12] *INAF, Osservatorio Astronomico di Bologna, via Ranzani 1, I-40127, Bologna, Italy*
[13] *INFN, Sezione di Bologna, viale Berti Pichat 6/2, I-40127, Bologna, Italy*
[14] *JPL, 4800 Oak Grove Dr., Pasadena, CA 91109, USA*
[15] *Universitá degli studi di Milano, Dip. di Fisica, via Celoria 16, 20133 Milano, Italy*

arXiv:1404.5633v2 [astro-ph.CO] 5 May 2014

6 May 2014

ABSTRACT

We report on the X-ray observation of a strong lensing selected group, SL2S J08544-0121, with a total mass of $2.4 \pm 0.6 \times 10^{14}$ $M_{\odot}$ which revealed a separation of 124 ± 20 kpc between the X-ray emitting collisional gas and the collisionless galaxies and dark matter (DM), traced by strong lensing. This source allows to put an order of magnitude estimate to the upper limit to the interaction cross section of DM of 10 cm^2 g^{-1}. It is the lowest mass object found to date showing a DM-baryons separation and it reveals that the detection of bullet-like objects is not rare and confined to mergers of massive objects opening the possibility of a statistical detection of DM-baryons separation with future surveys.

Key words: dark matter - X-rays:galaxies:clusters - gravitational lensing

1 INTRODUCTION

Merging galaxy clusters are unique astrophysical probes of the properties of dark matter (DM), which accounts for the majority of the mass in the universe. During a cluster merger, the cluster galaxies are collisionless particles, affected only by gravitational interactions, while the X-ray emitting plasma clouds, the dominant baryonic components in mass, are slowed down by ram pressure. Collisionless DM behaves as the galaxies so as the merging progresses the DM component is separated from the X-ray gas (Furlanetto & Loeb 2002). The presence of DM and constraints on its self-interaction cross section can therefore be inferred by measuring a spatial offset between the X-ray emission of the plasma and its total mass distribution as revealed by gravitational lensing, which is independent of the type of matter present.

An offset between the X-ray gas distribution and the mass inferred from gravitational lensing was detected for the first time in the Bullet cluster (Markevitch et al. 2004, M04 hereafter). A few other examples of 'bullet-like clusters' have been found following that discovery (e.g., Bradač et al. 2008; Merten et al. 2011; Dawson et al. 2012; Dahle et al. 2013). Since the collisions between two massive progenitors are rare (Shan et al. 2010) the number of detected massive

⋆ Based on observations obtained with XMM-Newton, an ESA science mission with instruments and contributions directly funded by ESA Member States and NASA.

† E-mail: gasta@lambrate.inaf.it

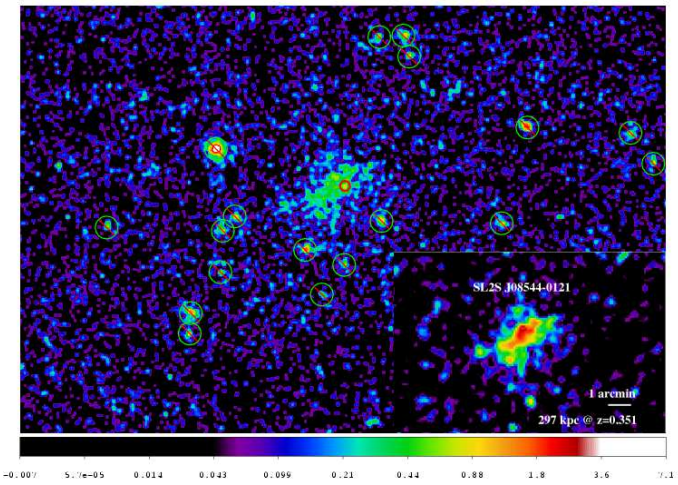

Figure 1. The EPIC 0.5-2 keV exposure-corrected and particle background subtracted image of SL2S J08544. The detected point sources are highlighted by the green circles; with the red circle of radius 11″ the point source within the group diffuse emission is also indicated. Point sources have been removed with the *CIAO* tool *dmfilth* which replaces photons within the source with a locally estimated background. This processed image of the diffuse emission is shown in the inset in the bottom right corner and it has been used to produce the X-ray contours shown in Fig.3. The image has been smoothed with a 7.5″ Gaussian (15″ for the inset). The color bar is in units of counts per pixel.

clusters undergoing mergers with the proper configuration is not expected to increase significantly. The utility of a small number of individual systems is limited by observational uncertainties in their collision velocity, impact parameter and angle with respect to the plane of the sky (e.g., Dawson 2013). Here we show that these studies can be extended to less massive systems which are much more numerous than massive clusters.

All distance-dependent quantities have been computed assuming a cosmological model with $\Omega_{\rm m}$=0.3, Ω_Λ=0.7 and H_0=70 km s^{-1} Mpc^{-1}.

2 THE OBJECT SL2S J08544-0121

The object SL2S J08544-0121 is a gravitational lens found in the Strong Lensing Legacy Survey (SL2S), a semi-automated search for strong lensing systems on the Canada-France-Hawaii Telescope Legacy Survey (CFHTLS) Deep and Wide fields (Cabanac et al. 2007). SL2S uses an algorithm aimed at detecting efficiently group scale lenses, with image separations of the order 3″-12″, intermediate between the ones found in galaxies (1″-2″) and massive clusters ($\gtrsim$20″) (More et al. 2012). We will therefore define SL2S J08544-0121 as a group based on this criterion. SL2S J08544 is located at redshift 0.35 and it displays a bimodal light distribution with a strong lensing system located at one of the two luminosity peaks separated by 54″ (267 kpc transverse physical distance). The strong lensing features detected from ground based images have been followed up with ACS camera on the *Hubble Space Telescope* (HST), revealing a very perturbed lensing configuration. Indeed, the main arc and the counter-image of the strong lensing system are located at $\sim$ 5″ and $\sim$ 8″ from the lens galaxy center respectively. It was found (Limousin et al. 2010) that a simple elliptical isothermal potential centered on the lensing galaxy could not satisfactorily reproduce the strong lensing observations. One straightforward way to measure the lensing model quality is to quote the RMS error which quantifies the distance between the observed position of the lensed images and the position derived from the lensing mass model. The smaller this distance, the better the mass model. For this model the RMS error in the image position is 0.38″. It was found that one needs to take into account in the modeling the mass distribution of the galaxy group within which the lens is embedded. In addition to the mass associated with the strong lensing deflector, mass associated with the second luminosity peak is required in order to accurately reproduce the strong lensing observations (RMS of 0.05″), demonstrating that SL2S J08544 displays a bimodal mass distribution following the light distribution. If on the contrary we construct a mass model where we add a mass clump consistent with the X-ray gas distribution (see Section 3) we are not able to improve the fit (RMS of 0.36″) with respect to the unsuccessful model where a single mass clump is associated with the SL deflector. The total mass of the group inferred from the strong lensing analysis is found to be in good agreement with an independent weak lensing analysis (Foëx et al. 2013). Spectroscopic follow-up of 18 ellipticals with FORS 2 at VLT confirms the presence of a galaxy group at $z = 0.35$ (Muñoz et al. 2013). In particular, the two brightest galaxies populating the two luminosity peaks are found at the same redshift. We do not confirm the bimodal distribution of velocities suggested in Muñoz et al. (2013): the redshift histogram has indeed a broad high velocity tail but a series of tests looking for departure from Gaussianity returned a null result. We applied a Anderson-Darling test (e.g., Hou et al. 2009) which returned a p value of 0.1553, therefore consistent with a Gaussian distribution. We also applied to the data the Kaye's Mixture Model (KMM) test (Ashman, Bird & Zepf 1994) which returned a p value of 0.06 for a two-group partition over a single group. The number of spectroscopic members does not allow a more detailed view of the merger dynamics and in particular the component of the velocity along the line of sight.

3 THE XMM OBSERVATION OF SL2S J08544-0121

We observed SL2S J08544-0121 with *XMM* as part of an X-ray follow-up program of the SL2S groups to obtain an X-ray detection of these strong-lensing selected systems and a measurement of the X-ray luminosity and temperature. SL2S J08544-0121 was observed by *XMM* for 9.5 ks for the MOS detector and 5 ks for the pn detector. The data were reduced with SAS v12.0.0 using the tasks *emchain* and *epchain*. We considered only event patterns 0-12 for MOS and 0 for pn and the data were cleaned using the standard procedures for bright pixels and hot columns removal and pn out-of-time correction. Periods of high backgrounds due to soft protons were filtered out but their impact was negligible for this observation. We checked the observation for contamination by solar wind charge exchange: ACE (Advanced Composition

Explorer) SWICS O+7/O+6 ratio was less than 0.3, a value which is typical of the quiescent Sun (Snowden et al. 2008). No variation in the light curve in the soft (0.5-2 keV) energy band was detected as a further check of negligible contamination by this background component.

For each detector we created images in the 0.5-2 keV band with point sources, detected using the task *edetect_chain*, masked using circular regions of 25″ radius centered at the source position. Point-source-free, cleaned images have been generated with the *CIAO* tool *dmfilth* which replaces photons within the source with a locally estimated Poisson-deviated noise. The images have been exposure corrected and background subtracted using the XMM-Extended Source Analysis Software (ESAS). The *XMM* image in the 0.5-2 keV band of the field of SL2S J08544-0121 is shown in Fig.1. The X-ray emission of SL2S J08544-0121 is clearly extended: the best-fit β-model to the surface brightness profile has a core radius of $r_c = 128^{+64}_{-49}$ kpc ($26''^{+13}_{-10}$) and $\beta = 0.52^{+0.09}_{-0.06}$. The faint point source (a 3σ detection) in the SW embedded within the extended emission of the group has been replaced within a circle of 11″ radius with a locally estimated Poisson noise with the same procedure adopted for the other point sources in the image. This is the largest region not overlapping with the peak of the emission itself (and corresponding roughly to 60% of the encircled energy fraction, EEF, for a point source on-axis). We estimate that the possible contamination by the emission in the wings of the PSF corresponds to 1% of the extended emission. The *XMM* astrometry is known to be accurate to within 1″ (Guainazzi 2013) and we quantified the error in the determination of the peak by calculating the error in the position of the center of a two-dimensional beta model fitted in a region of 30″ radius (80% of the EEF) with the CIAO software *Sherpa* (Freeman, Doe & Siemiginowska 2001) which is of the order 3″. We therefore estimate the error in the position of the X-ray peak to be 4″. If instead of replacing the weak point source we model it with an appropriate PSF model we obtain the same position for the X-ray peak within the errors.

To assess if the possible systematic error due to undetected source might be larger than the above estimate, we tested our analysis on simulations of 10^3 *XMM* images with a source list with flux distribution and source density computed using the Log (N) - Log(S) from Moretti et al. (2003) down to a level of 1×10^{-17} ergs cm^{-2} s^{-1} and we then added the extended emission of the source; the main instrumental characteristics (PSF, vignetting, background) were taken into account. The standard deviation of the distribution of position of peaks was 3″, consistent with the estimated error.

For spectral fitting, we extracted spectra for each detector from a 1.5′ aperture centered on the peak of the emission, with radius chosen to maximize the S/N over the background. Redistribution matrix files (RMFs) and ancillary response files (ARFs) were generated using the SAS tasks *rmfgen* and *arfgen* in extended source mode. The spectra from the three detectors were jointly fitted with an APEC thermal plasma (Smith et al. 2001) modified by Galactic absorption (Kalberla et al. 2005). The spectral fitting was performed with *Xspec* (Arnaud 1996) in the 0.5-12 keV band (0.5-13 keV for the pn) using the C-statistic and quoted metalicities are relative to the abundances of Grevesse & Sauval (1998).

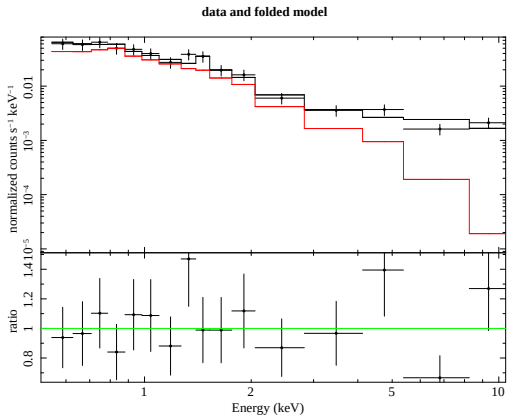

Figure 2. pn spectrum extracted from a 1.5′ aperture: all the background components, instrumental and cosmic, have been modeled and the source component is shown by the solid red line. The ratio of data over the model are also shown.

To account for the background we included additional spectral components in the fits: we included two APEC components (kT = 0.07 keV and 0.2 keV, the former un-absorbed) to account for the Galactic foreground and a power law component ($\Gamma = 1.41$) for the Cosmic X-ray Background due to unresolved AGNs. To account for the instrumental background, we included a number of Gaussian lines and a broken power law models, which were not folded through the ARF. The background parameters were constrained by fitting spectra extracted from an annular region close to the source extraction region and in a larger annulus of 10′-12′ and then the fitted normalizations were rescaled accordingly to the source extraction area. The estimated 0.5-2 keV background is in good agreement with the ROSAT All-sky Survey (RASS) spectrum obtained using the X-ray Background Tool (Snowden et al. 1997). We obtained a fit with a C stat/dof value of 31/36 and the best fit parameters are kT $= 3.5^{+0.6}_{-0.5}$ keV and $Z = 0.6^{+0.7}_{-0.5}$ $Z_\odot$. We show in Fig.2 the pn spectrum and the best fit model, highlighting the source component. As a further check to the maximum likelihood fitting we use Markov chain Monte Carlo (MCMC) techniques and Bayesian inference in *Xspec* to constrain the confidence level of the temperature determination. We allowed for a 10% systematic in our background modeling setting Gaussian priors on the rescaled normalizations of the cosmic and particle background with a width of 10% of their best fit values and we set constant priors on the source parameters. We produced a chain of length 10^4 steps, after an initial "burn-in" of 5000 steps, with the Metropolis-Hastings sampler. We then marginalized over the all other parameters to generate a posterior probability for the temperature. The 68% confidence interval is (3.0, 4.5) keV.

For the total mass determination of the system we used the chain outputs for the temperature parameter as inputs in the M-T scaling relation of Arnaud, Pointecouteau & Pratt (2005) obtained for the full sample investigated in that paper and within an over-density of 200: we find an estimate for the mass of the system of $M_{200} = 2.4 \pm 0.6 \times 10^{14}$ $M_\odot$ which is in good agreement with the lensing determination of $M_{200} = 2.2^{+0.4}_{-0.6} \times 10^{14}$ $M_\odot$, derived adopting the value of dispersion velocity, 644^{+69}_{-102} km s^{-1}, of the Single Isothermal

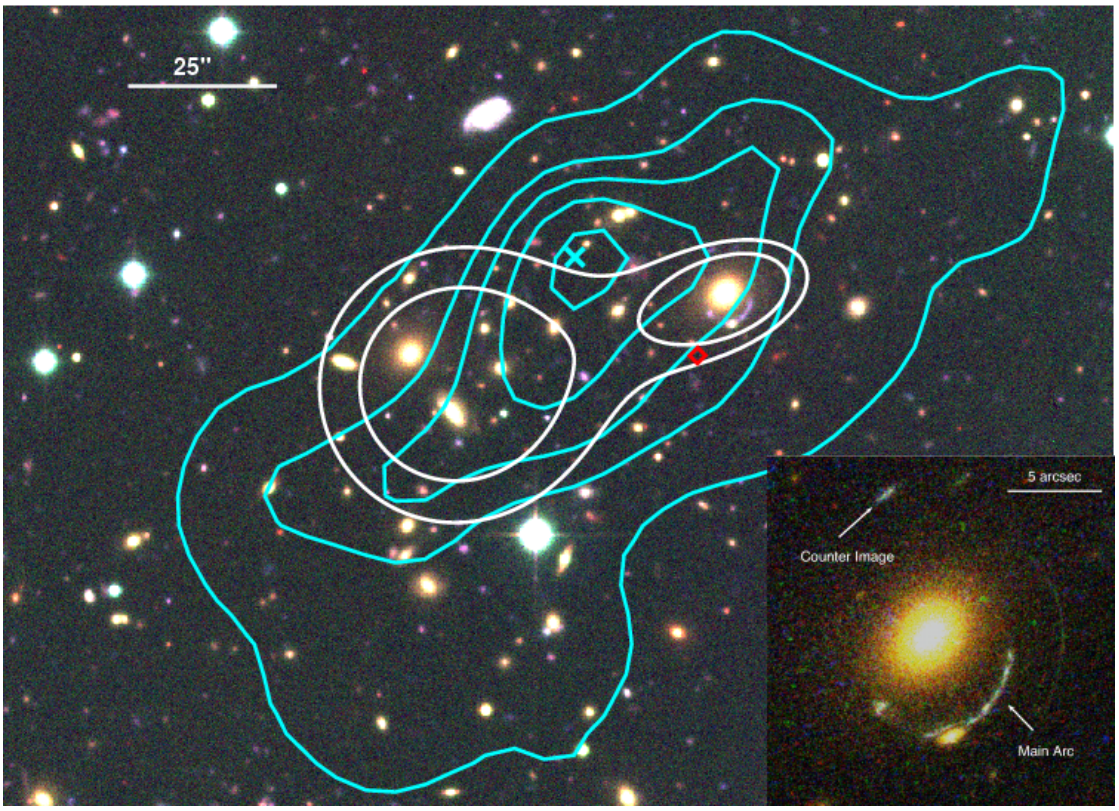

Figure 3. Composite CFHTLS g,r,i color image of the group SL2S J08544-0121, with a size of $3' \times 2'$ corresponding to 891 kpc × 594 kpc at the redshift of the object, z=0.351. Overlayed in white are the mass contours derived from the strong lensing model, showing where the projected mass density equals $(1.5, 2.0) \times 10^{10}$ $M_\odot$ arcsec^{-2}. The X-ray contours from the *XMM* observation are over-plotted in cyan, showing the clear displacement between the X-ray peak, marked by the cyan x point, and the lensing mass, centered at the coordinates of the galaxy populating the lens (see insert). The red diamond point marks the position of the excluded point source discussed in the text. The insert in the bottom right corner shows the HST image with the main arc and its counter image, revealing the particular asymmetric configuration.

Sphere model used in the modeling of the weak lensing data (Foëx et al. 2013). Simulations indicate that clusters even in the middle of a major merger follow the M-T relation with a scatter of about 20%-25% along the mass axis (e.g., Rasia et al. 2011).

4 DM-BARYONS SEPARATION

The X-ray data reveal a single peak located between the two light/mass clumps with a clearly extended and disturbed morphology and an elongation of the emission along the South-East direction. These features are typical of an advanced merger event with the two clumps having already experienced their first passage following a South-East North-West direction. The geometry of an elongated single X-ray feature between the two DM clumps revealed by lensing is analogous to the configuration seen in the cluster MACS J0025.4-1222 (Bradač et al. 2008). The peak of the baryonic mass distribution derived from the X-ray emission is offset by $25'' \pm 4''$ from the strong lensing system in the North-West, corresponding to a transverse physical separation of 124 ± 20 kpc at the redshift of the object and given our adopted cosmology (see Fig.3.)

The mass estimate of $M_{200} = 2.4 \pm 0.6 \times 10^{14}$ $M_\odot$ makes SL2S J08544-0121 the smallest mass system found to date for which a significant DM-baryons separation has been detected, ~ 7 times less massive than the Bullet cluster and ~ 2 times less massive than the "Burst" cluster, ZWCl 1234.0+02916 (Dahle et al. 2013), the currently known smallest mass system showing a bullet-cluster like configuration.

Using the data of SL2S J08544-0121 we can derive another independent order-of-magnitude estimate for the self-interaction cross section of DM. We follow the first argument of M04 and assume that the NW subcluster has passed once close to the center of the SE subcluster and that the direction of motion is very nearly in the plane of the sky. The offset between the DM centroid of the NW subcluster and the peak of the X-ray gas, which is assumed to belong originally to the same structure, indicates that the scattering depth of the DM subcluster with respect to the collisions of the DM particle stream is lower than 1. If this would not be the case, the DM would behave as a fluid showing ram pressure stripping as the gas. We further assume that the surface mass density along the collision direction is similar to that along the line of sight: this is a conservative estimate given the best fit ellipticity of the halo from strong lensing (0.50 ± 0.04, Limousin et al. 2010). The scattering depth of DM in the strong lensing subcluster is therefore

$$\tau = \frac{\sigma}{m}\Sigma < 1 \quad (1)$$

where σ is the DM collision cross section, m is its particle mass, and Σ is the DM surface density of the NW subcluster associated to the lens. The choice of the radius where to calculate the average DM surface density in previous studies has been selected to provide conservative constraints and a comparison between different cluster systems. A radius of 150 kpc was used for the subcluster of the Bullet cluster given the available lensing data at that time (M04) and then used as a reference in following studies. If we calculate Σ at the position of the strong lensing peak averaged over a radius of 150 kpc we obtain 0.06 g cm^{-2} and therefore an estimate for the upper limit on the scattering cross section of $\sigma/m \lesssim 17$ cm^2 g^{-1}. If instead we use a radius smaller than the measured separation of 124 kpc, in particular 100 kpc, we get 0.10 g cm^{-2} and an upper limit of $\sigma/m \lesssim 10$ cm^2 g^{-1}.

The detection of DM-baryons separation in SL2S J08544-0121 provides further evidence for the collisionless DM model and an independent upper limit on its interaction cross section. Systems with mass of $1-2\times10^{14}$ M$_\odot$ like the Bullet Group are 10^3 times more numerous than massive clusters of 1×10^{15} M$_\odot$ like the Bullet Cluster and therefore examples of DM-baryons separation are not as rare as usually assumed (Amendola et al. 2013). Indeed numerical simulations already suggested a fair number of "bullets" at every mass scale (e.g. Forero-Romero, Gottlöber & Yepes 2010), in particular the number of bullet groups is three times larger than the one of bullet clusters (Fernandez-Trincado et al. 2014). Upcoming lensing surveys (e.g. with the *Euclid* satellite) and X-ray surveys (with the *eROSITA* telescope on the Spektrum-Roentgen-Gamma Mission) should therefore provide hundreds of similar examples allowing the properties of DM to be studied in a statistical manner (Massey, Kitching & Nagai 2011).

5 CONCLUSIONS

SL2S J08544-0121 is a really remarkable object because it is a strong lensing selected group, its lensing image configuration already provided evidence of a bimodal mass configuration and the X-ray follow-up showed evidence of baryons-DM separation down to at least a mass scale of few times 10^{14} M$_\odot$. It might be considered as a proof of concept of the potential of upcoming deep lensing and X-ray surveys of discovering many similar examples allowing a statistical study of the properties of DM. Deeper X-ray observations with *Chandra* and optical spectroscopy of an increased number of member galaxies are needed for a better understanding of the merger geometry of this system.

ACKNOWLEDGMENTS

FG is supported by INAF-ASI through grant I/023/05/0, I/088/06/0 and I/032/10/0. AF is supported by INAF VIPERS PRIN 2008/2010. V.M. is supported by FONDECYT 1120741. R.M. is supported by FONDECYT 3130750. R.C., G.F., M.L., V.M. is supported by ECOS-CONICYT C12U02. TV is supported by CONACYT through grant 165365 and 203489. MM is supported by ASI/INAF/I/023/12/0 and from INFN project PD51.

REFERENCES

Amendola L. et al., 2013, Living Rev. in Relativity, 16, 6
Arnaud K. A., 1996, in ASP Conf. Ser. 101: Astronomical Data Analysis Software and Systems V, Vol. 5, p. 17
Arnaud M., Pointecouteau E., Pratt G. W., 2005, A&A, 441, 893
Ashman K. M., Bird C. M., Zepf S. E., 1994, AJ, 108, 2348
Bradač M., Allen S. W., Treu T., Ebeling H., Massey R., Morris R. G., von der Linden A., Applegate D., 2008, ApJ, 687, 959
Cabanac R. A. et al., 2007, A&A, 461, 813
Dahle H. et al., 2013, ApJ, 772, 23
Dawson W. A., 2013, ApJ, 772, 131
Dawson W. A. et al., 2012, ApJ, 747, L42
Fernandez-Trincado J. G., Forero-Romero J. E., Foëx G., Verdugo T., Motta V., 2014, ApJ, accepted, arXiv:1404.5636
Foëx G., Motta V., Limousin M., Verdugo T., More A., Cabanac R., Gavazzi R., Muñoz R. P., 2013, A&A, 559, A105
Forero-Romero J. E., Gottlöber S., Yepes G., 2010, ApJ, 725, 598
Freeman P. E., Doe S., Siemiginowska A., 2001, in Astronomical Society of the Pacific Conference Series, Vol. 238, Astronomical Data Analysis Software and Systems X, Harnden Jr. F. R., Primini F. A., Payne H. E., eds., p. 483
Furlanetto S. R., Loeb A., 2002, ApJ, 565, 854
Grevesse N., Sauval A. J., 1998, Space Science Reviews, 85, 161
Guainazzi M., 2013, XMM-SOC-CAL-TN-0018
Hou A., Parker L. C., Harris W. E., Wilman D. J., 2009, ApJ, 702, 1199
Kalberla P. M. W., Burton W. B., Hartmann D., Arnal E. M., Bajaja E., Morras R., Pöppel W. G. L., 2005, A&A, 440, 775
Limousin M. et al., 2010, A&A, 524, A95+
Markevitch M., Gonzalez A. H., Clowe D., Vikhlinin A., Forman W., Jones C., Murray S., Tucker W., 2004, ApJ, 606, 819, M04
Massey R., Kitching T., Nagai D., 2011, MNRAS, 413, 1709
Merten J. et al., 2011, MNRAS, 417, 333
More A., Cabanac R., More S., Alard C., Limousin M., Kneib J.-P., Gavazzi R., Motta V., 2012, ApJ, 749, 38
Moretti A., Campana S., Lazzati D., Tagliaferri G., 2003, ApJ, 588, 696
Muñoz R. P. et al., 2013, A&A, 552, A80
Rasia E., Mazzotta P., Evrard A., Markevitch M., Dolag K., Meneghetti M., 2011, ApJ, 729, 45
Shan H., Qin B., Fort B., Tao C., Wu X.-P., Zhao H., 2010, MNRAS, 406, 1134
Smith R. K., Brickhouse N. S., Liedahl D. A., Raymond J. C., 2001, ApJ, 556, L91
Snowden S. L. et al., 1997, ApJ, 485, 125
Snowden S. L., Mushotzky R. F., Kuntz K. D., Davis D. S., 2008, A&A, 478, 615